RSC Advances

ROYAL SOCIETY OF CHEMISTRY

www.rsc.org/advances

Obtaining information about valuable metals in computer and mobile phone scraps using laser-induced breakdown spectroscopy (LIBS)

*Francisco W. B. Aquino, Jozemir M. Santos, Rodrigo R. V. Carvalho, Jomarc A. R. Coelho and Edenir R. Pereira-Filho**

Grupo de Análise Instrumental Aplicada (GAIA), Departamento de Química (DQ), Universidade Federal de São Carlos (UFSCar), PO Box 676, Zip code 13565-905, São Carlos, SP, Brazil.

*Corresponding author: erpf@ufscar.br

Phone: +55 16 3351-8092

Fax: +55 16 3351-8350

Keywords

Laser-induced breakdown spectroscopy (LIBS), e-waste, gold, silver, computer scraps, mobile phones, printed circuit board.

Abstract

The constant projected increase in electronic-waste (e-waste) generation coupled with the high costs of several raw materials employed by the electronics industry are factors that justify studies regarding new analytical methodologies suitable for applications in recycling centers, industrial facilities and academic laboratories. Longer preparation routines for sample analysis and the diverse physical and chemical characteristics of these materials are challenges frequently encountered during the development of analytical procedures. In this work, laser-induced breakdown spectroscopy (LIBS) was applied to the direct investigation of Au and Ag in computer scraps and in the electromagnetic shielding of mobile phone housings. The results show that this technique can be a useful tool for obtaining information regarding the profiles of these elements at the surface and in the bulk of these materials without preparation steps and for semi-quantitatively evaluating Ag in the type of samples analyzed.

Introduction

During the last twenty years, the amount of electronic waste (or e-waste) generated has increased dramatically[1,2], and this trend is currently projected to continue for the next several years. Some of the main factors that have led to this situation are the constant technological advances that quickly turn a piece of high-technological equipment into an obsolete object within a short period of time.[2]

This scenario is worrying and complex because the correct and efficient management of these residues, which have significant pollution potential, involves legal, technological and economic challenges for both developed and developing nations.[3] An example of this phenomenon is the large number of international routes for illegally dumping e-waste from developed nations into Southeast Asia and countries in Africa.[4]

Factors including the high demand for the valuable raw materials (e.g., Au, Ag and Pd) used in the electronics industry, the limited number of natural sources of these elements and the actions of environmental protection agencies explain the increase of "green" initiatives. These initiatives for recycling can mitigate the environmental and human health problems arising from improper e-waste management.[5,6]

To enable the recycling of metals from e-waste with efficiency and economic viability, several processes have been proposed or improved in recent years.[7–10] This trend of employing ecological approaches to handle residues intended to be recycled, including e-waste, is also being extended to analytical methods.[11]

The development of green analytical methods is not always trivial.[12] However, laser-induced breakdown spectroscopy (LIBS) is an emerging analytical technique that possesses great potential for this application.[13,14]

In this sense, Solo-Gabriele *et al.*[15] proposed the use of LIBS for the on-line detection of copper arsenate in wood. Unnikrishnan *et al.*[16] used LIBS to classify plastics and Xia and Bakker[17] to classify moving-waste materials in concrete recycling. In materials that compound with e-waste, Stepputat and Noll[18] employed LIBS for the on-line detection of hazardous metals and brominated flame retardants in polymers. Between 2013 and 2015, Aguirre *et al.*[19], Aquino and Pereira-Filho[20] and Carvalho *et al.*[21] used LIBS to investigate scraps of mobile phones.

The LIBS technique offers additional advantages, such as real-time multi-elemental analysis, no or minimal sample preparation, good spatial and depth resolution, the elimination of expensive gases for plasma formation, low residue production with minimal sample destruction and it is possible to detect low atomic number elements like C, O, Be, Li and N. In addition, compact system are nowadays available for field and industrial applications[22,23].

Some limitations of LIBS are the lack of availability of matrix-matched standards for many applications and its relatively low sensitivity and precision compared to those of other spectrophotometric techniques, such as inductively coupled plasma optical emission spectrometry (ICP OES).[24–26]

Taking all of the aspects of the potential of LIBS into consideration, we here present an application of this technique for the direct investigation of Au and Ag in computer and mobile-phone scraps.

Wang and Gaustad[5] used a weighted-sum model to investigate the trade-offs among economic value, energy-saving potential, and eco-toxicity; they concluded that Au has the highest recovery priority for end-of-life printed circuit boards (PCBs). According to Tuncuk *et al.*[27], computer PCBs can contain up to 250 g/ton Au, which is significantly high: 25–250 times higher compared to gold ores that contain approximately 1–10 g/ton Au.[27] For Ag Wang and

Gaustad[5] have noted that the recovery priority of Ag from PCBs is lower than that of other elements because of the small energy saving *per* ton of waste PCBs. In this sense, in addition to the environmental aspects, improving the efficiency of the recycling process of e-waste (not solely for Ag) is one of the main reasons that several studies are currently in progress for this type of residue.[6,8,9,28]

Experimental

Samples

The presence of Au was investigated in 36 broken or obsolete computer components (G1–G36) selected because of their golden color and their applications as electric signal conductors in the contacts of computer components (exceptions were samples G8, G9 and G36, which were selected solely because of their applications as conductors of electrical signals in memory boards). These criteria were selected because, in many places, e-waste is sorted without specific knowledge (e.g., recycling points in poor countries or small companies that merely classify e-waste and sell it to large recyclers). The presence of Ag was investigated in 13 mobile phones (S1–S13) with plastic housings that exhibited a rigid internal layer with a ceramic aspect (see Fig. 1) used as electromagnetic shielding. A description of the samples is given in Table 1.

LIBS setup

The LIBS spectra were obtained using a J200 LIBS system (Applied Spectra, Fremont, CA, USA) managed by the Axiom 2.5 software. This instrument is equipped with a nanosecond Nd:YAG laser, which can provide up to 100 mJ in a single pulse at 1064 nm and at a frequency of 10 Hz. The plasma light emission was recorded using a 6-channel CCD spectrometer with a

fixed gate width of 1.05 ms, in a spectral window from 186 to 1042 nm, resulting in spectra composed of 12,288 points (variables). The samples were positioned in the ablation chamber system by an automated XYZ stage and using a 1280 × 1024 CMOS color camera imaging system. A HEPA air cleaner connected to the ablation chamber was used to purge ablated particles from the laser/sample interaction. The emission lines were identified using the Aurora software (Applied Spectra).

LIBS and scanning electron microscopy analyses

After the computer components (G1–G36) were disassembled and the housings were cut from the mobile phones (S1–S13), the obtained samples were directly analyzed without any chemical pretreatment. To avoid undesirable signals in the LIBS spectra resulting from contamination of the samples by dust or handling, a surface cleanup was performed at each ablation point (5 points *per* sample) using a single pulse with an energy of 10 mJ in a 250 micrometer spot. Immediately after this procedure, each sample was analyzed under the following conditions. For the Au samples (G1-G36, Table 1), the laser power was adjusted to 75 mJ, the spot size was reduced to 75 μm, and the gate delay was set to 0.5 μs. Afterwards, 10 pulses *per* point were fired. For the Ag samples (S1-S13, Table 1), the laser power was 100 mJ, the spot size was 125 μm, and the gate delay was set to 1.0 μs. Finally, 30 pulses *per* point were fired. The entire procedure of laser positioning and focalization was controlled by the Axiom 2.5 software. A representation of the analytical process is shown in Fig. 1.

Semi-quantitative information from representative samples was obtained using a scanning electron microscope equipped with an energy-dispersive X-ray spectroscopy unit (SEM-EDS; INSPECT S50, FEI Company, Hillsboro, OR, USA) operated at 25.0 kV.

Data collection and chemometric evaluation

The spectral data from the samples interrogated for the presence of Au and Ag were separately analyzed. Each raw data set was normalized by its individual norm and subsequently mean-centered. Afterwards, the two data sets were organized into distinct matrices from which chemometric analyses were performed or derived. The matrix for the Au samples contained 1,800 rows × 12,288 columns (36 samples × 5 points *per* sample × 10 pulses = 1,800 spectra with 12,288 wavelengths). The matrix for the Ag samples contained 1,950 rows × 12,288 columns (13 samples × 5 points *per* sample × 30 pulses = 1,950 spectra with 12,288 wavelengths). Matlab 2009a (MathWorks, Natick, MA, USA) was used for the data processing.

Results and discussion

The studied samples did not formally indicate the presence of Au or Ag, and both data sets were initially inspected through principal component analysis (PCA). Because a general profile for the distribution of the investigated metals along the bulk of samples is also desirable, PCA was performed using matrices organized with the average spectra *per* laser pulse. From the original matrices, the average of the 5 points of each sample was calculated, resulting in new matrices with 360 rows × 12,288 columns (36 averaged spectra × 10 pulses) and 390 rows × 12,288 columns (13 averaged spectra × 30 pulses) for the Au and Ag samples, respectively. From these matrices, the average of each sample was calculated, resulting in matrices with 10 rows × 12,288 columns and 30 rows × 12,288 columns for the Au and Ag samples, respectively.

The score plots for the PCAs are presented in Fig. 2a for the Au and in Fig. 2b for the Ag samples. The variance explained by the first and second principal components (PCs) for the samples where Au was investigated was 98.5% (PC1 = 82.9; PC2 = 15.6%), whereas in the case

of the coated polymers where Ag was investigated, the variance explained was 97.9% (PC1 = 88.4; PC2 = 9.5%).

Analysis of the score plot in Fig. 2a revealed a prominent segregation of pulse 1, P1 (as a function of its PC1 value) relative to the other pulses. Because the numbers 1 to 10 represent the laser pulse sequence in the samples, a remarkable difference clearly exists between the surface and bulk of the samples. Analysis of the loadings for PC1 (Fig. 3) revealed a strong correlation between Au and the surface (information at pulse 1, P1) of the analyzed samples because the Au emission lines exhibited remarkable negative values in PC1. Moreover, the deeper pulses (P3–P10) are characteristic of Cu and Ni (with positive loading values).

For the coated polymers (Ag, P1–P30), the score plot (Fig. 2b) also shows remarkable differences between the surface (accessed by the first pulses, P1 and P2) and the bulk (P3-P30). Furthermore, the changes along the pulse increments are not as abrupt as the changes observed for the Au samples. In addition to the different interactions between the laser and the materials of the two sample groups, other possible reasons for this difference are a greater thickness or greater homogeneity of the material. On the basis of the loadings for PC1and PC2 (see Figs. 4 and 5), both situations appear to occur. Except for the emission lines at 328.06 and 338.28 (nm), the signals for Ag present negative loadings for PC1 (Fig. 4), whereas Ag is mainly responsible for the positive loadings for PC2 (Fig. 5).

Still, on the basis of the loading values for PC1 (Fig. 4), the polymeric layer is inferred (in general terms) to be hit starting from the fifteenth pulse (P15). This observation takes into account that the distribution of scores starting from P15 is related to positive loadings for PC1 and negative loadings for PC2 (see Figs. 4 and 5), where the influence of Ag decreases and those of C, Ca, CN, H, N, O and Ti increase. These elements are strongly associated with polymers

used in mobile phones [20]. The micrograph shown in Fig. 1 is an example of a sample where the coating layer was pierced and the polymer was hit.

After the presence of Au and Ag was confirmed in the sample sets, the Aurora software and literature data were used to select variables (emission lines) according to their emissions intensities.[29] The selected emission lines, in increasing order of wavelength, were 208.20 (II), 242.79 (I), 267.59 (I), 280.20 (II), and 479.25 (I) for Au; and 243.78 (II), 328.06 (I), 338.28 (I), 520.90 (I), 546.54 (I), and 547.15 (I) for Ag. After this selection process, new PCA calculations were performed for the two sets of samples.

Figure 6a shows the emission profile of the first through the tenth pulse, considering all of the Au samples (an average of five ablation points) at the selected wavelengths. In the score plot (Fig. 6b) obtained from the PCA performed with the selected variables, the explained variance for PC1 (97.74) plus PC2 (1.97) was 99.71%. In addition, a progressive reduction of the distances between the subsequent scores was observed from the first through the tenth pulse, whereas the values of this score increased along the PC1 axis. On the basis of the wavelengths selected and the remarkable segregation in the score of the first pulse (P1), Au was inferred to be basically located at the surface of the samples. After the seventh pulse (P7), the differences among the Au emissions were observed to be minimal, probably because of the low content or absence of Au in the deeper layers of most of the samples. However, no quantitative value related to the thickness of the samples could be determined on the sole basis of this score plot.

To improve the understanding of the Au content in the analyzed samples, a new PCA was performed using a matrix formed by the average spectra of each sample and using the same variable selection. Each spectrum used in this analysis was obtained by averaging 50 spectra (5 points *per* sample, 10 pulses *per* point). Through the score plot from this PCA shown in Fig. 6c,

the explained variance of PC1 (47.43) plus PC2 (32.14) = 79.56%; in addition, a distribution pattern exists for the scores of the samples from the negative to the positive values of PC2. This behavior along the PC2 axis is mainly related to the emissions at 267.59 nm. In relation to the score dispersion along the PC1 axis, all of the selected wavelengths are strongly related to its negative values. On the basis of these observations, in general terms (in the surface and the bulk), the Au concentration is higher in the samples with positive values for PC2 and negative values for PC1, i.e., in samples G7, G29 and G25 (see the loading plot for PC2 in Fig. 1S of the supplementary information).

The segregation of samples G8, G9 and G36 in the group where the Au signal was minimal or absent was not entirely surprising. Despite the fact that these samples originated from computer components where Au is normally present, these pieces did not exhibit the golden color observed for the others (see Fig. S2 in the supplementary information).

To test these hypotheses, a third PCA was carried out with the same variable selection; however, in this case, only the spectra obtained by the average of the first pulse for each of the five ablation points were used (the score plot presented in Fig. 6d was compared with that obtained for the bulk, Fig. 6c). Additionally, the samples were classified according to their emission intensities for the first, fifth and tenth pulses at 267.59 nm (see Fig. 7), and representative samples resulting from the classification based on the first pulse segregation were analyzed by SEM-EDS (see Table 2).

A comparison of the score plot of the new PCA (see Fig. 6d; explained variance of PC1 (55.80) plus PC2 (19.38) = 75.18%) with the previous PCA (Fig. 6c) reveals that the segregation of samples G8, G9 and G36 remains. However, when only the surface signal is considered (Fig. 6d), the samples with higher responses for Au present positive values for PC1 (e.g. samples G7,

G23 and G25). This result is confirmed by the concentration of Au at the surfaces of samples G7, G23, G25 and G27, which were analyzed by SEM-EDS (see Table 2), and also noticeable by the black squares (pulse 1) in Fig. 7, which shows the normalized emission signal (267.59 nm) for the first (black squares), fifth (circle) and tenth (triangle) laser pulses.

With respect to Fig. 7, even if the laser interacts differently with materials with distinct characteristics, the fact that all of the samples are metallic alloys with similar qualitative compositions (see Table 2) contributes to credibility of the variations of the sample emission intensities, and consequently the changes in the positions of samples for the different number of pulses, point out the samples where the Au layer is thicker.

Examples of this observation include the behavior of sample G25, which remains between the samples with higher emissions, in opposition to the behaviors of samples G23 and G24, which exhibit decreased emissions. Also interesting are the behaviors of samples G18 and G20, which exhibited increased emissions between the first and fifth pulses and showed higher signals in the internal layers.

The higher scattering among the score values along the PC1 axis of Fig. 6d when compared to Fig. 6c occurs due to the wide range of Au content at the surface of the samples. Again, this observation is verified by the results presented in Table 2 (where the samples analyzed were selected according to the emission intensities of the first pulse).

Also with respect to Table 2, even though the SEM-EDS data obtained for the surfaces of the selected samples show a direct quantitative correlation between the emission signal of first laser pulse (from the LIBS analysis) and the Au concentration at the sample surface is not possible, some points deserve consideration.

Samples where Au is absent or observed in concentrations lower than 15% (e.g., G9 and G33) can quickly be identified without the necessity of expensive or laborious procedures. The main reason for the lack of a strong correlation between the LIBS and SEM-EDS data was likely the wide variation in the thickness of the samples. This type of information can be used in screening procedures that aiming the identification of samples with similar characteristics in e-waste management centers or for research purposes in academic institutions.

Despite this variation, the LIBS technique can provide data for comparing the relative thickness of the Au layers of different samples; it can also provide data related to whether the investigated element is located at the surface or in the bulk of the sample, e.g., the behaviors of samples G18 and 20 where emission intensity increases according to the increment of laser pulses (for G18, the intensity was practically the same at the fifth and tenth pulses). This type of information cannot be easily obtained using other techniques. The results obtained by energy-dispersive X-ray fluorescence spectroscopy (EDXRF), which was our first option for comparing the LIBS data presented in this manuscript, corroborate our previous results. As evident in Fig. S3 of the supplementary information, for these analyses, the dimensions of the various samples were smaller than the minimum required for EDXRF measurements with the equipment used here (Shimadzu model EDX 700); in addition, the thickness of the Au and Ag coatings of several samples was problematic because the spectra obtained showed the samples as being uniform instead of what they really were (i.e., pieces coated with metal oxides or different metallic layers).

For the samples where the presence of Ag was investigated, the same chemometric approach was applied. Initially, using the selected wavelengths (Fig. 8a), PCA was performed considering the average spectra obtained for each laser pulse.

The resulting score plot is shown in Fig. 8b (explained variance of PC1 (80.4) plus PC2 (17.6) = 98.0%). In relation to the same analysis performed with all of the variables (Fig. 2b), the information obtained from the score profile does not show substantial differences. This similarity occurs despite the inversion of the score distribution along the PC2 axis. At the PC1 axis, the scores of the first pulses retain negative values, and the inflection point also remains between the scores of Pulses 9 and 11. These results highlight the influence of Ag for the characterization of these samples. Note that the distribution profile of the scores practically does not change and that the explained variance of the PCA without the variable reduction was practically the same: 97.9% compared with 98.0% for the PCA performed with the variable selection. This procedure can be used not solely to identify the Ag presence in electromagnetic shielding of mobile phones or from other communication devices, but also to infer the main elements present in other materials used for the same purpose.

Regarding the PCAs performed using the average spectra of all of the pulses (Fig. 8c) and the average spectra obtained only for the first pulse (Fig. 8d), the segregation of sample 12 (S12) is immediately noticeable in both score plots. This segregation occurs because of the absence of Ag in the coating layer of this sample. Another particular feature of this sample is the presence of chromium in its internal layer (see Table 3 and Fig. S4 in the supplementary information). Nevertheless, this information would not be available if the analyses were performed using only SEM-EDS.

As observed from the comparison of the LIBS and SEM-EDS data for the Au samples, the correlation between the results provided by these techniques for the Ag samples using the average emission of the first pulse was not suitable for quantitative determinations. However, in this case, in addition to the differences in the thicknesses of the layers that contain Ag, the

different particle sizes of the surface layers likely contribute significantly to the decrease of the correlation data obtained from these two techniques (see Fig. S5 in the supplementary information). Even taking into account the influence of the previously discussed variables and considering the concentration range where Ag was detected in the samples (53.8 to 67.5%; see Table 3 and Fig. 9), we reasonably conclude that LIBS can be useful for the semi-quantitative determination of Ag for this type of sample.

The Fig. 9 shows the normalized emissions intensity for the average of the first pulse fired in each of the five ablation points in the samples where Ag was analyzed. The small increments at the emission intensity can justify the differences observed between the increase in the response order for Ag in the LIBS analysis and in the concentration determined from SEM-EDS analysis.

Concerning the possibility of using Ag as a unique descriptor for providing information related to the manufacturer or origin of the mobile phone, the results of the PCAs performed do not support this application. Tables 1s and 2s of supplementary information shows the Relative Standard Deviation for the selected emission lines for Au (Table 1s) and Ag (Table 2s). In these tables it is observed that the average RSD ranged from 19.6 to 27.6 for Au and from 16.4 to 35.4 for Ag.

Regarding the %RSD for the golden samples, is important to consider that for 267.59 nm (λ used for building the Fig. 7) the value of maximum %RSD (84.1%) was obtained for sample G20. As shown in Figure 7, in the sample G20, Au is located in its bulk and not in its surface (see the increment signal from pulse 1 to pulse 10), this observation justifies high %RSD not only at 267.59 nm, but also in others wavelength. The reasons for the high %RSD observed in other samples (see G13, G14) may be related to its low emission signal, probably due to its thin

304 layer in the sample surfaces. On the other hand, the samples with high Au content (see G7, G23,
305 G25 and G27 in Table 2 and Fig. 7) showed %RSD lower than average values for all
306 wavelengths. For silver samples (Table 2s) the wavelengths 520.9 and 546.54 showed the lowest
307 %RSD, these values are in accordance with the general data reported for LIBS.
308
309 **Conclusions**

310 Despite the challenges that involve calibration for accurate quantification by LIBS, its use
311 for the direct evaluation of Au and Ag in scraps of computer and mobile phones presented in this
312 manuscript is a quick tool, applicable especially in situations where superficial inspection is not
313 sufficient to determine the presence and estimate the concentration of these elements (mainly for
314 Ag in the electromagnetic shielding of mobile phones).
315 Furthermore, the possibilities for obtaining information about the distribution of elements
316 on the surface and in the bulk of samples for this type of sample is a noticeable advantage when
317 compared with other techniques such as SEM-EDS (which is expensive) or EDXRF. In addition,
318 the application of the previously described procedures for use with portable systems expands the
319 possibilities of LIBS technique applications.
320
321 **Acknowledgments**

322 The authors are grateful for the financial support of Conselho Nacional de
323 Desenvolvimento Científico e Tecnológico, CNPq (grants 304772/2012-7, 401074/2014-5 and
324 474357/2012-0), to Grants 2012/01769-3, 2012/50827-6 and 2013/04688-7 São Paulo Research
325 Foundation (FAPESP) and to Prof. Newton de Almeida Silva from Reciclagem Tecnológica de
326 São Carlos (Reciclatesc) for supplying the samples.

References

1 F. O. Ongondo, I. D. Williams and T. J. Cherrett, *Waste Manag.*, 2011, **31**, 714–730.

2 P. Kiddee, R. Naidu and M. H. Wong, *Waste Manag.*, 2013, **33**, 1237–1250.

3 C. R. Oliveira, A. M. Bernardes and A. E. Gerbase, *Waste Manag.*, 2012, **32**, 1592–1610.

4 J. Li, B. N. Lopez, L. Liu, N. Zhao, K. Yu and L. Zheng, *Waste Manag.*, 2013, **33**, 923–934.

5 X. Wang and G. Gaustad, *Waste Manag.*, 2012, **32**, 1903–1913.

6 P. M. H. Petter, H. M. Veit and A. M. Bernardes, *Waste Manag.*, 2014, **34**, 475–482.

7 D. Pant, D. Joshi, M. K. Upreti and R. K. Kotnala, *Waste Manag.*, 2012, **32**, 979–990.

8 F. Wang, J. Huisman, C. E. M. Meskers, M. Schluep, A. Stevels and C. Hagelüken, *Waste Manag.*, 2012, **32**, 2134–2146.

9 L. Jing-ying, X. Xiu-li and L. Wen-quan, *Waste Manag.*, 2012, **32**, 1209–1212.

10 Y. He and Z. Xu, *RSC Adv.*, 2015, **5**, 8957–8964.

11 C. Bendicho, I. Lavilla, F. Pena-Pereira and V. Romero, *J. Anal. At. Spectrom.*, 2012, **27**, 1831–1857.

12 M. de la Guardia and S. Garrigues, *Challenges in Green Analytical Chemistry*, Royal Society of Chemistry, Cambridge, 1st edn., 2011.

13 C. Pasquini, J. Corttez, L. M. C. Silva and F. B. Gonzaga, *J. Brazilian Chem. Soc.*, 2007, **18**, 463–512.

14 D. Santos, L. C. Nunes, G. G. A. De Carvalho, M. D. S. Gomes, P. F. De Souza, F. D. O. Leme, L. G. C. Dos Santos and F. J. Krug, *Spectrochim. Acta - Part B At. Spectrosc.*, 2012, **71-72**, 3–13.

15 H. M. Solo-Gabriele, T. G. Townsend, D. W. Hahn, T. M. Moskal, N. Hosein, J. Jambeck and G. Jacobi, *Waste Manag.*, 2004, **24**, 413–424.

16 V. K. Unnikrishnan, K. S. Choudhari, S. D. Kulkarni, R. Nayak, V. B. Kartha and C. Santhosh, *RSC Adv.*, 2013, **3**, 25872–25880.

17 H. Xia and M. C. M. Bakker, *Talanta*, 2014, **120**, 239–247.

18 M. Stepputat and R. Noll, *Appl. Opt.*, 2003, **42**, 6210–6220.

19 M. A. Aguirre, M. Hidalgo, A. Canals, J. A. Nóbrega and E. R. Pereira-Filho, *Talanta*, 2013, **117**, 419–424.

20 F. W. B. Aquino and E. R. Pereira-Filho, *Talanta*, 2015, **134**, 65–73.

21 R. R. V. Carvalho, J. A. O. Coelho, J. M. Santos, F. W. B. Aquino, R. L. Carneiro and E. R. Pereira-Filho, *Talanta*, 2015, **134**, 278–283.

22 F. J. Fortes and J. J. Laserna, *Spectrochim. Acta - Part B At. Spectrosc.*, 2010, **65**, 975–990.

23 B. Noharet, C. Sterner, T. Irebo, J. Gurell, A. Bengtson, H. Karlsson and E. Illy, *Proc. SPIE 9369, Photonic Instrum. Eng. II.*, 2015, 1–7.

24 R. E. Russo, X. Mao, J. J. Gonzalez, V. Zorba and J. Yoo, *Anal. Chem.*, 2013, **85**, 6162–6177.

25 D. W. Hahn and N. Omenetto, *Appl. Spectrosc.*, 2012, **66**, 347–419.

26 D. A. Cremers and R. C. Chinni, *Appl. Spectrosc. Rev.*, 2009, **44**, 457–506.

27 A. Tuncuk, V. Stazi, A. Akcil, E. Y. Yazici and H. Deveci, *Miner. Eng.*, 2012, **25**, 28–37.

28 R. Cayumil, R. Khanna, M. Ikram-Ul-Haq, R. Rajarao, A. Hill and V. Sahajwalla, *Waste Manag.*, 2014, **34**, 1783–1792.

29 S. Legnaioli, G. Lorenzetti, L. Pardini, V. Palleschi, D. M. D. Pace, F. A. Garcia, R. Grassi, F. Sorrentino, G. Carelli, M. Francesconi, F. Francesconi and R. Borgogni, *Spectrochim. Acta Part B At. Spectrosc.*, 2012, **71-72**, 123–126.

List of Figures

Table 1. Description of samples (component type, coded manufacturer, origin country, production year).

Sample code	Component type	Manufacturer	Origin country	Production year	Sample code	Component type	Manufacturer	Origin country	Production year
G1	Contact of desktop memory	A	-	2004	G26	Motherboard connector	-	-	-
G2	Contact of desktop memory	B	China	-	G27	WiFi board connector	G	China	-
G3	Contact of desktop memory	A	-	-	G28	Motherboard connector	-	-	-
G4	Contact of notebook memory	C	Japan	1997	G29	Motherboard connector	-	-	-
G5	Contact of notebook memory	C	Japan	1997	G30	Motherboard connector	-	-	-
G6	Contact of notebook memory	C	Japan	1997	G31	Motherboard connector	-	-	-
G7	Contact of notebook memory	D	China	-	G32	Motherboard connector	-	-	-
G8	Contact of desktop memory	-	-	1998	G33	Motherboard connector	-	-	-
G9	Contact of desktop memory	-	-	-	G34	Motherboard connector	-	-	-
G10	Contact of desktop memory	B	USA	-	G35	Motherboard connector	-	-	-
G11	Pin of desktop processor	E	Philippines	2000	G36	Contact of desktop memory	H	China	-
G12	Pin of desktop processor	E	Philippines	2000	S1	Mobile phone cover housing	I	Brazil	-
G13	Pin of desktop processor	E	Philippines	2000	S2	Mobile phone cover housing	D	Brazil	-
G14	Pin of desktop processor	E	Philippines	2000	S3	Mobile phone cover housing	D	Brazil	-
G15	Pin of desktop processor	E	Costa Rica	2000	S4	Mobile phone cover housing	I	Brazil	2003
G16	Pin of desktop processor	F	Malaysia	2001	S5	Mobile phone cover housing	J	Brazil	2006
G17	Pin of desktop processor	-	-	-	S6	Mobile phone cover housing	D	South Korea	-
G18	Pin of desktop processor	F	Malaysia	1999	S7	Mobile phone cover housing	D	South Korea	2006
G19	Pin of desktop processor	E	Philippines	2000	S8	Mobile phone cover housing	D	Brazil	-
G20	Pin of desktop processor	E	-	1995	S9	Mobile phone cover housing	D	Brazil	-
G21	Pin of desktop processor	E	-	-	S10	Mobile phone cover housing	I	Brazil	2006
G22	Pin of desktop processor	-	-	-	S11	Mobile phone cover housing	D	Brazil	-
G23	Pin of desktop processor	E	Malaysia	1999	S12	Mobile phone cover housing	D	Brazil	-
G24	Pin of desktop processor	E	-	-	S13	Mobile phone cover housing	D	Brazil	-
G25	Motherboard connector	-	-	-					

Table 2. Weight percent profile* (RSD) of the majority elements detected in the selected Au samples analyzed by SEM-EDS.

Sample	Weight (%) of detected elements, as determined by SEM-EDS analysis																		
	Surface of the sample									Inside the crater resulting from LIBS analysis									
	Au	C	Cu	Fe	Ni	O	P	Pb	Sn	Au	C	Cu	Fe	Ni	O	P	Pb	Sn
G9	-	-	37.30 (0.2)	-	-	5.17 (3.8)	-	5.56 (2.7)	51.97 (0.1)	-	-	86.91 (0.1)	-	-	0.96 (40)	-	-	12.13 (0.8)
G33	11.26 (21)	28.43 (21)	7.96 (1.2)	-	22.69 (0.2)	29.66 (12)	-	-	-	-	-	-	-	-	-	-	-	-
G10	15.72 (11)	26.97 (41)	-	-	40.77 (0.2)	16.55 (35)	-	-	-	-	20.86 (115)	37.50 (0.2)	-	22.10 (0.4)	10.40 (69)	9.14 (10.2)	-	-
G2	19.73 (1.3)	29.22 (7.2)	-	-	39.40 (0.1)	11.66 (15)	-	-	-	-	51.27 (2.6)	47.30 (0.1)	-	1.42 (4.3)	-	-	-	-
G28	29.57 (6.6)	19.20 (87)	1.83 (17)	-	49.40 (0.1)	-	-	-	-	-	-	73.84 (0.3)	-	26.16 (1.2)	-	-	-	-
G27	48.60 (1.1)	28.00 (26)	-	-	6.34 (7.5)	17.07 (39)	-	-	-	-	23.31 (111)	23.85 (0.4)	-	29.76 (0.2)	9.47 (97)	13.61 (4.9)	-	-
G23	64.48 (1.5)	-	-	3.47 (20.6)	32.05 (0.5)	-	-	-	-	42.74 (3.4)	-	-	5.66 (6.2)	51.60 (0.2)	-	-	-	-
G25	92.50 (0.7)	-	-	-	7.5 (6.5)	-	-	-	-	21.41 (18)	-	18.63 (1.0)	-	59.96 (0.1)	-	-	-	-
G7	95.14 (0.8)	-	-	-	4.86 (18)	-	-	-	-	20.60 (6.9)	19.00 (50)	-	-	41.88 (0.1)	18.53 (16)	-	-	-

* Average of the measurements performed at three different points for each analyzed sample.

Table 3. Weight percent profile* (RSD) of the majority elements detected in the selected Ag samples analyzed by SEM-EDS.

Sample	Weight (%) of detected elements. as determined by SEM-EDS analysis											
	Surface of the sample						Inside the crater resulting from LIBS analysis					
	Ag	Al	C	Cr	Mg	O	Ag	Al	C	Cr	Mg	O
S12	-	13.44 (4.59)	5.39 (594)	-	81.17 (0.02)	-	-	5.56 (6.7)	14.70 (29)	0.59 (6.5)	59.96 (0.03)	19.18 (2.65)
S1	53.77 (0.13)	-	28.10 (3.64)	-	1.65 (140)	16.47 (3.32)	56.57 (0.12)	-	26.09 (3.95)	-	1.51 (169)	15.83 (31)
S10	61.42 (0.10)	-	23.46 (4.37)	-	1.93 (103)	13.20 (3.85)	3.13 (3.55)	-	77.78 (0.48)	-	0.38 (1083)	18.81 (19)
S8	62.31 (0.11)	-	21.51 (5.35)	-	1.38 (215)	14.80 (3.68)	51.33 (0.11)	-	31.94 (2.44)	-	1.28 (184)	15.98 (25)
S4	67.43 (0.11)	-	19.92 (6.35)	-	1.94 (118)	10.71 (4.54)	64.98 (0.11)	-	21.45 (5.89)	-	2.02 (114)	11.56 (59)
S9	67.75 (0.10)	-	19.00 (6.51)	-	1.99 (104)	11.27 (4.35)	68.10 (0.10)	-	17.90 (7.30)	-	1.82 (131)	12.19 (51)

* Average of the measurements performed at three different points for each analyzed sample.

Figure 1

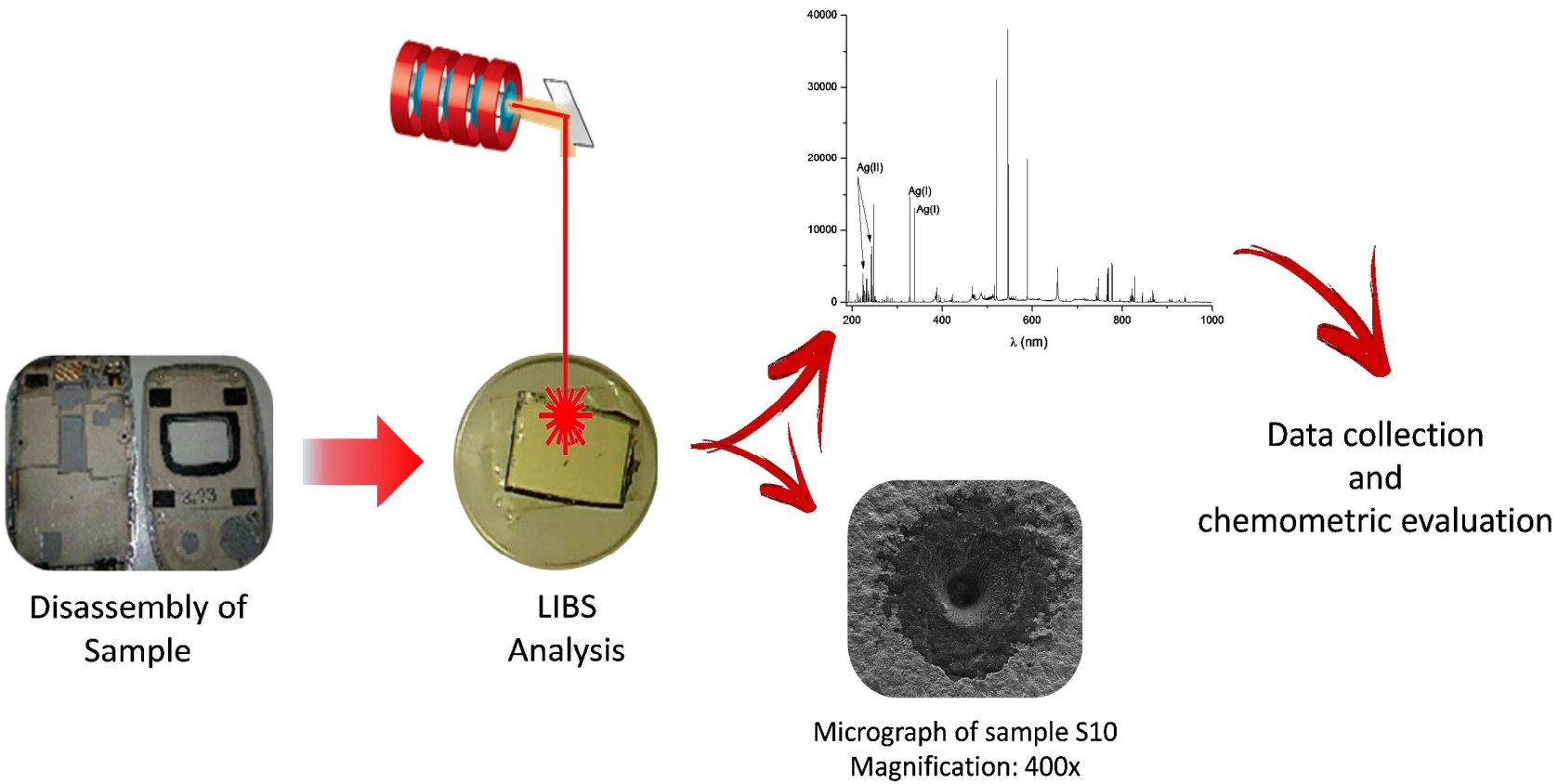

Figure 2

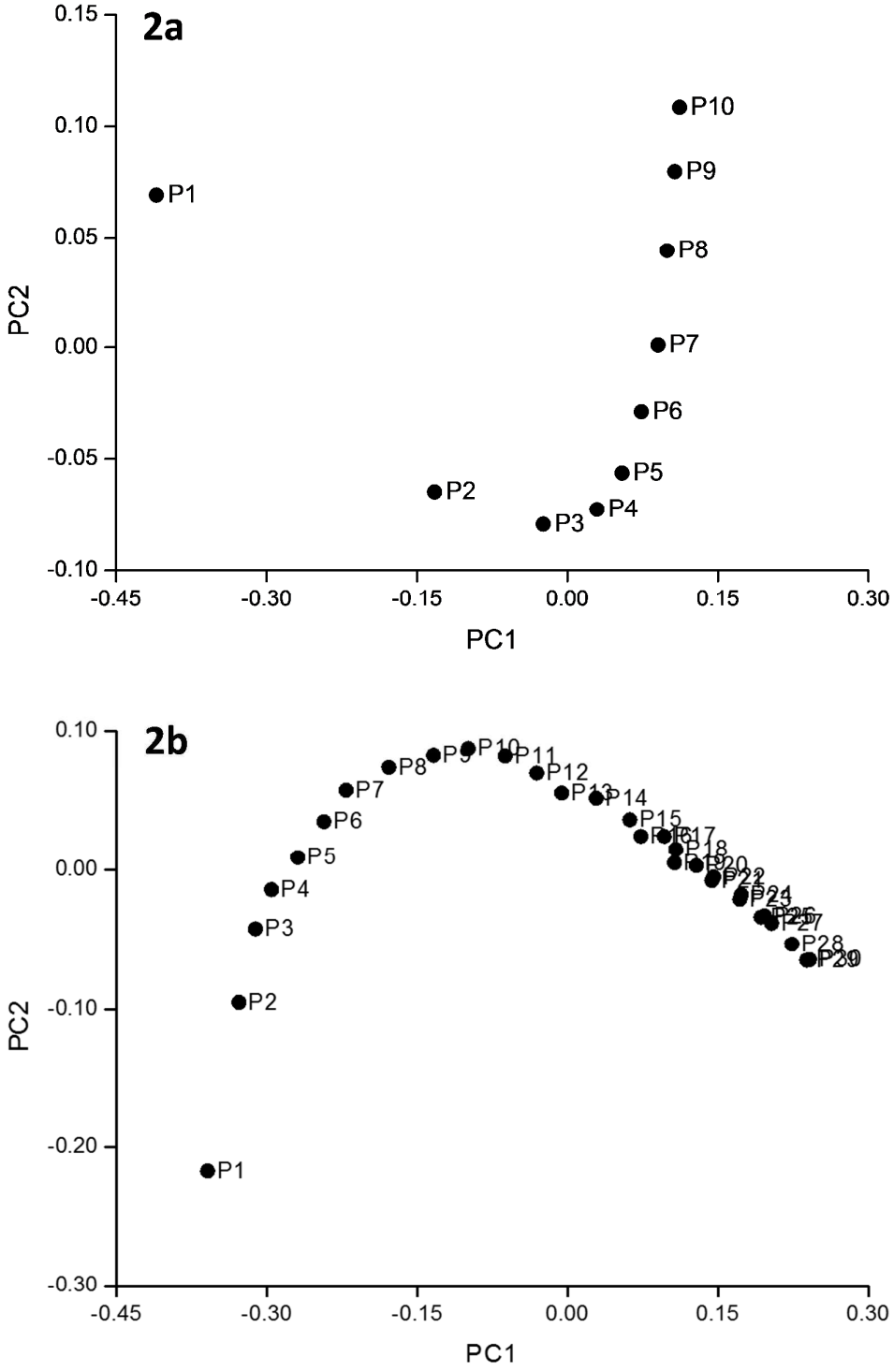

Figure 3

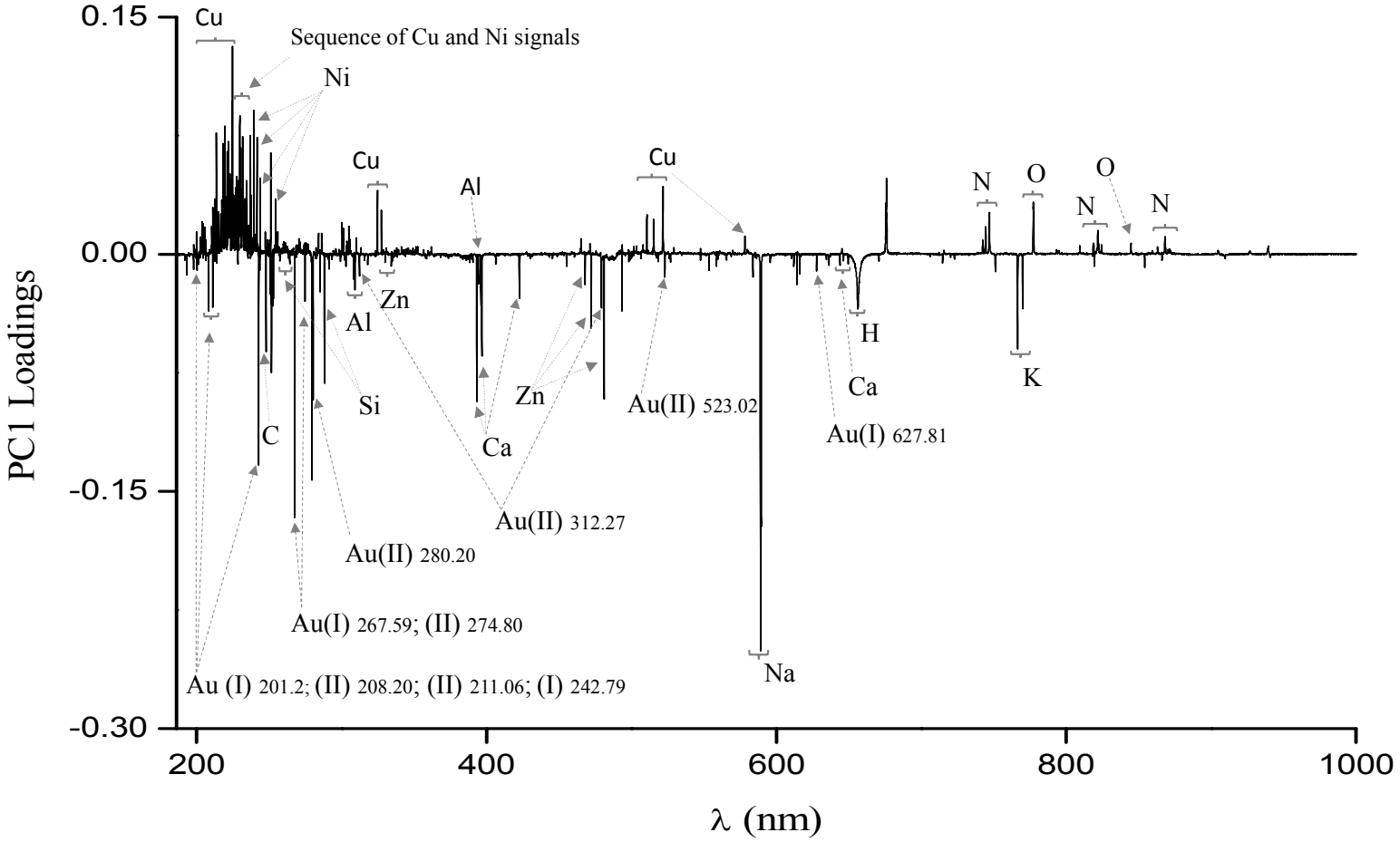

Figure 4

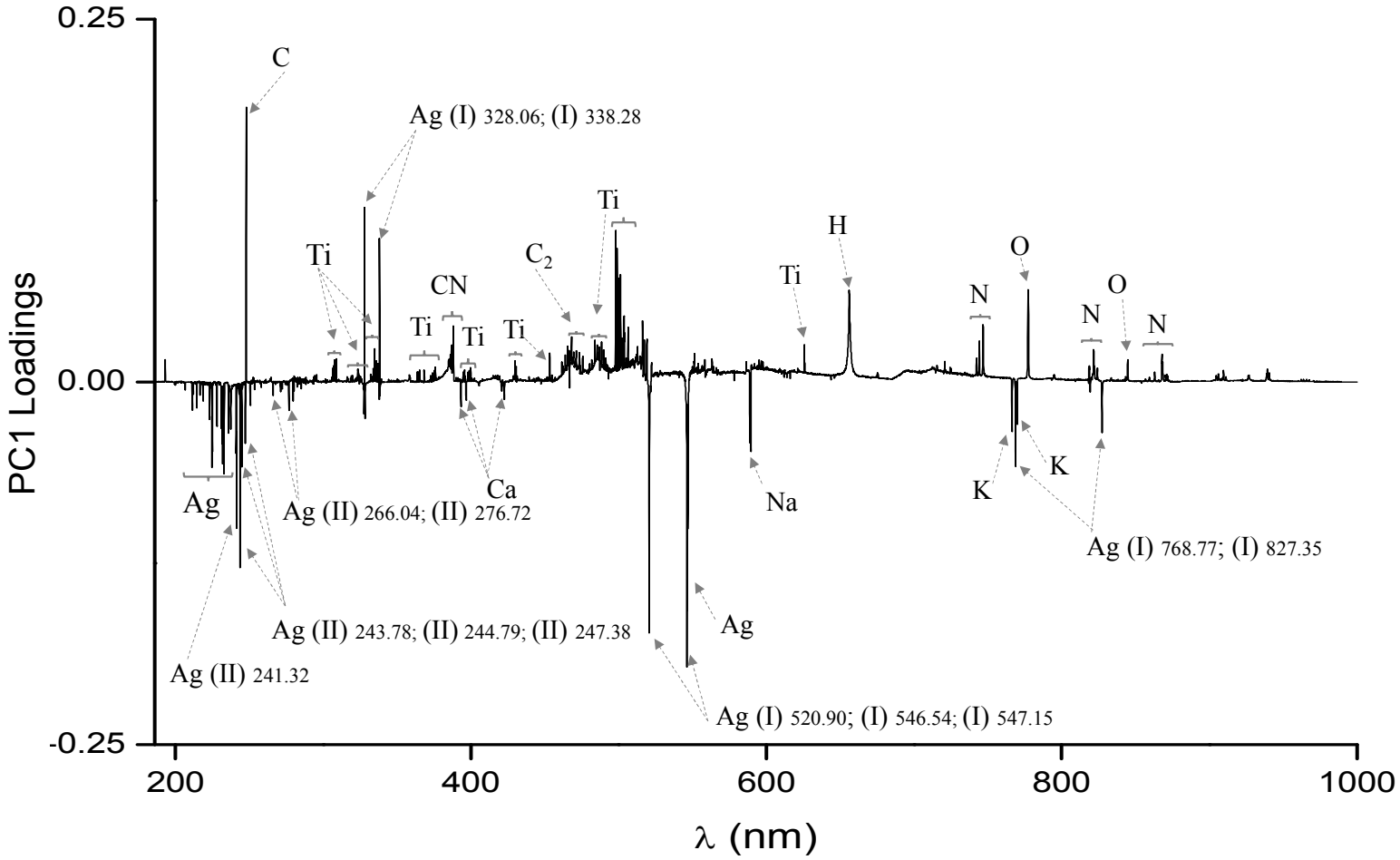

Figure 5

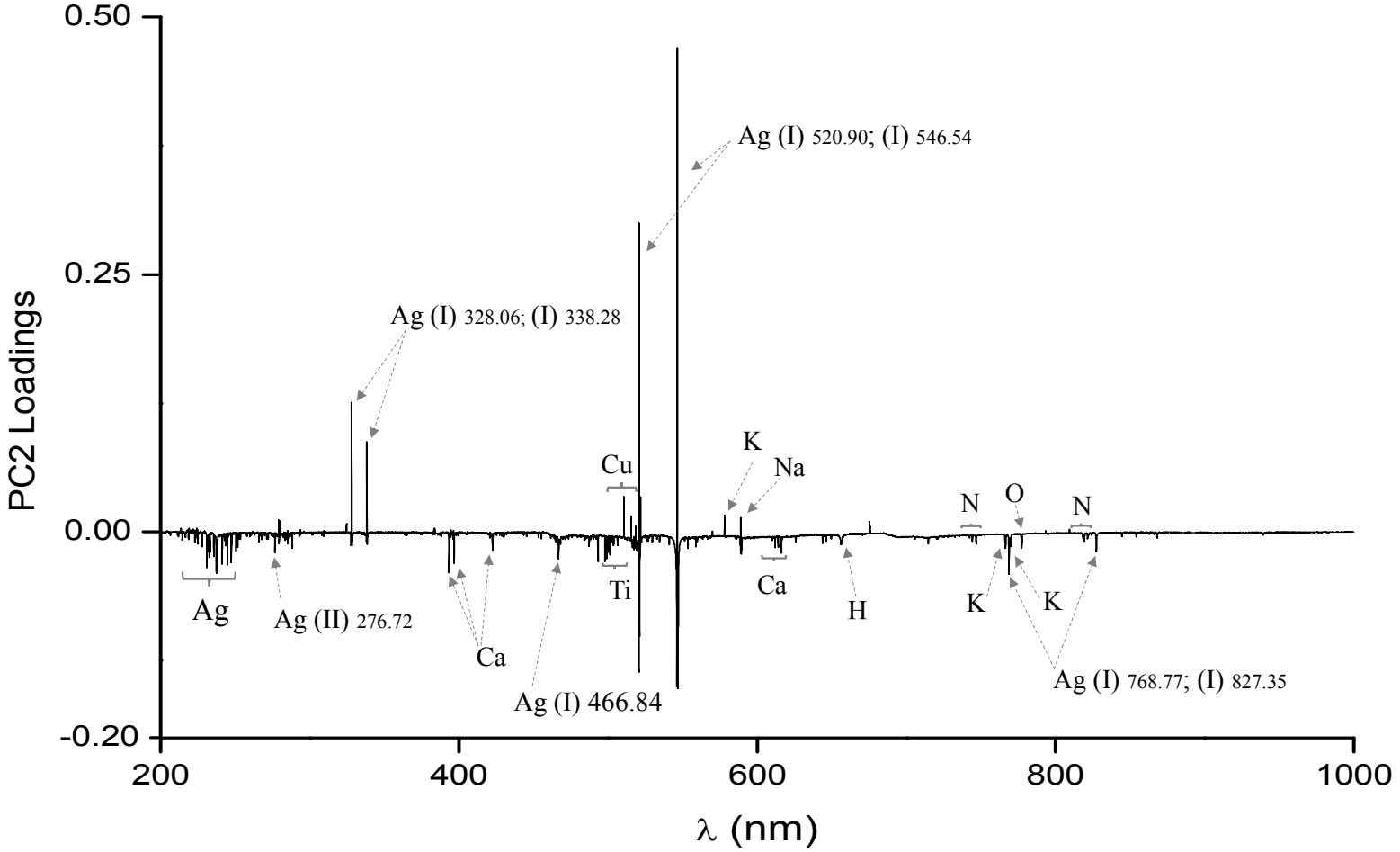

Figure 6

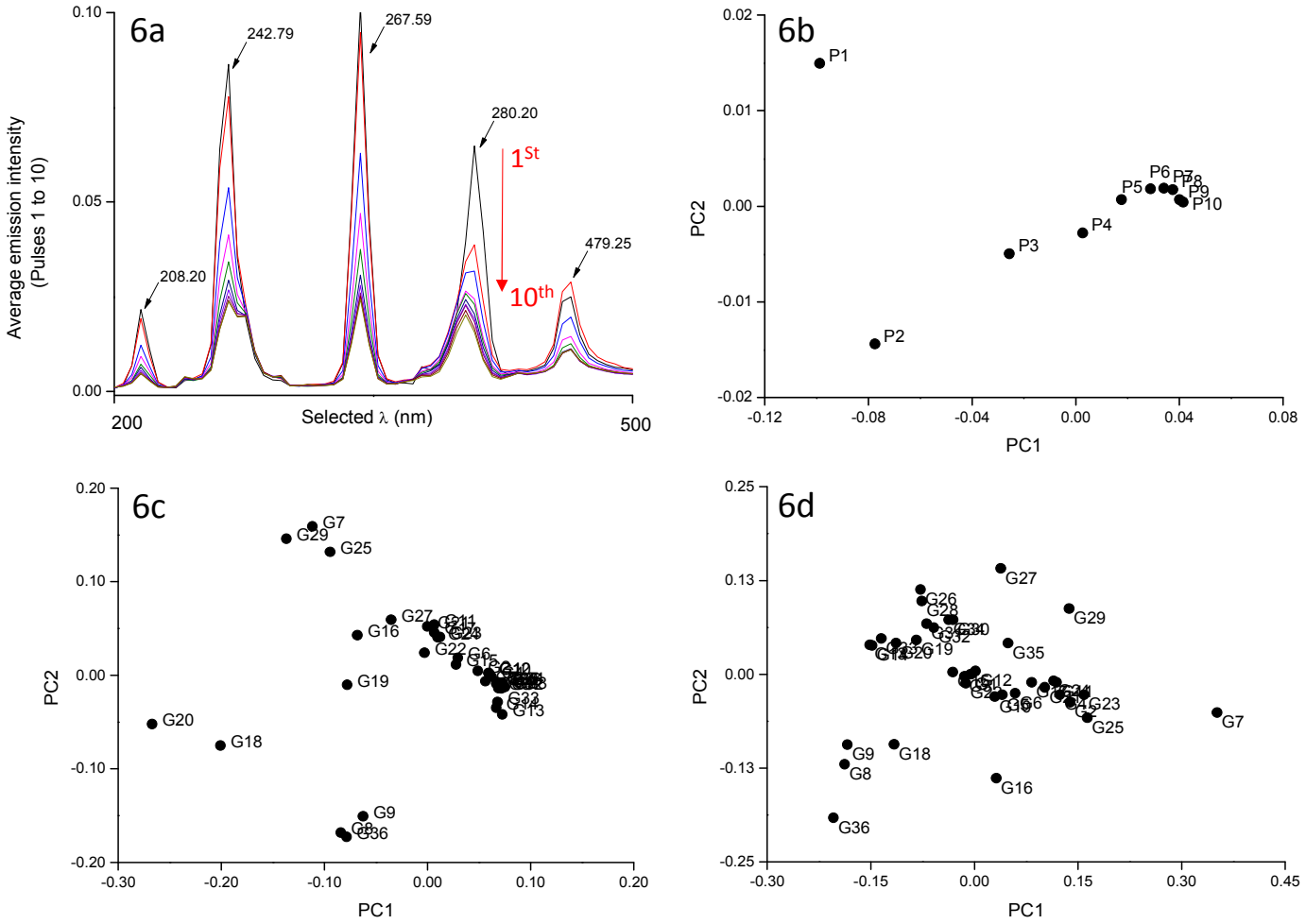

Figure 7

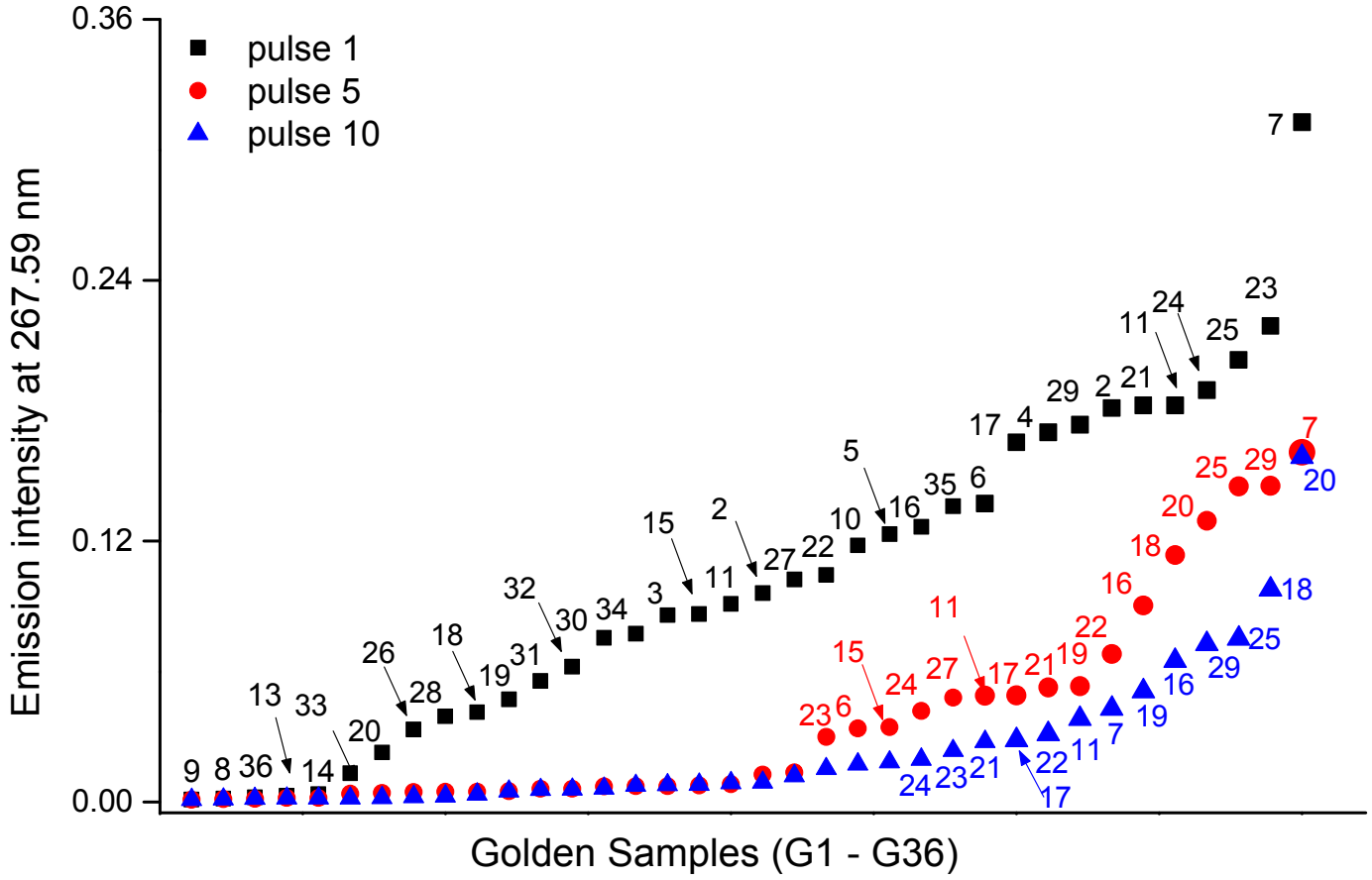

Figure 8

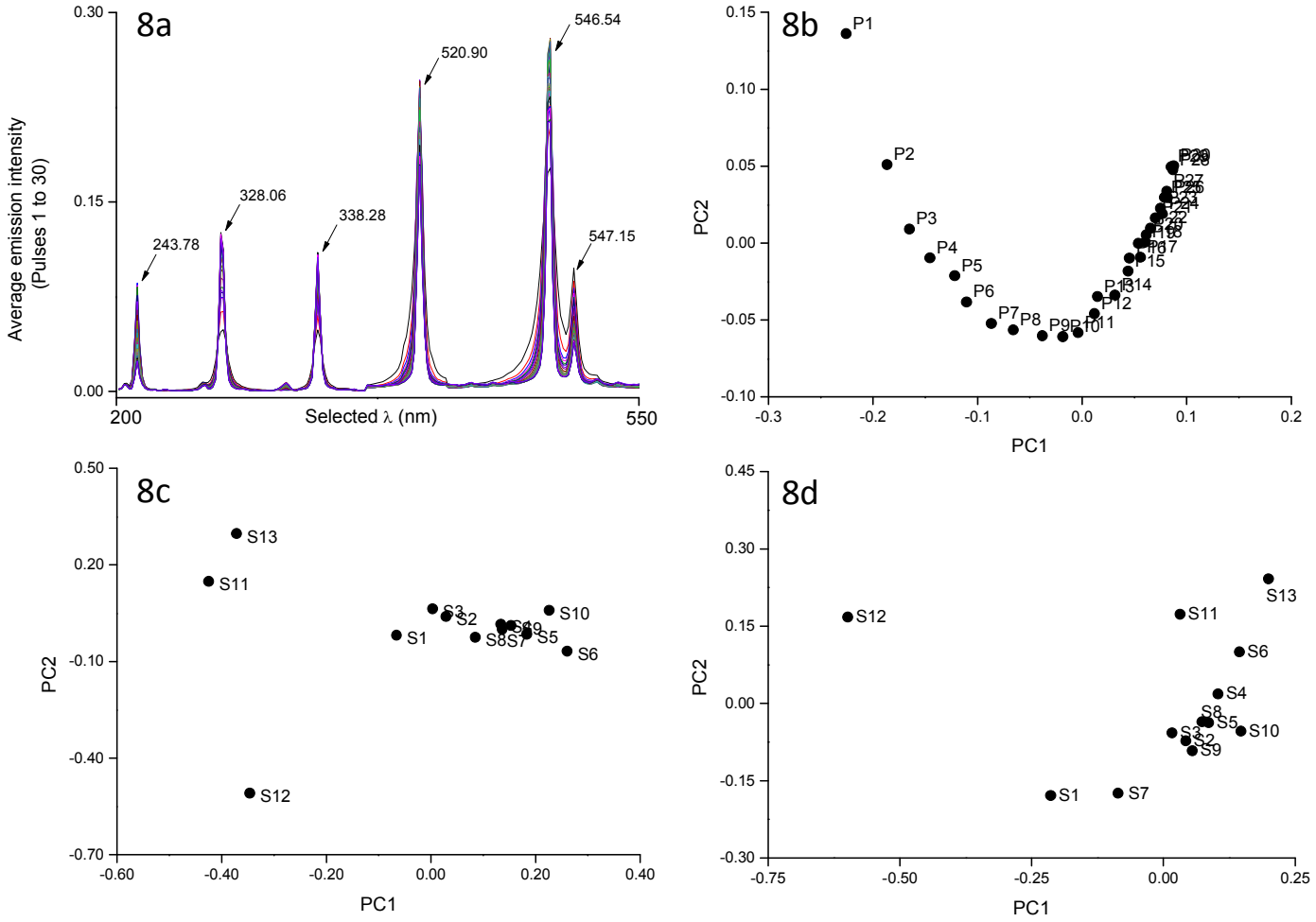

Figure 9